Acta Pharmaceutica Sinica B 2025;15(5):2764–2777

Chinese Pharmaceutical Association
Institute of Materia Medica, Chinese Academy of Medical Sciences

Acta Pharmaceutica Sinica B

www.elsevier.com/locate/apsb
www.sciencedirect.com

ORIGINAL ARTICLE

Marine-derived new peptaibols with antibacterial activities by targeting bacterial membrane phospholipids

Shang Chen[a,†], Dong Liu[a,†], Liyang Wang[b], Aili Fan[a], Mengyue Wu[a], Ning Xu[c], Kui Zhu[b,*], Wenhan Lin[a,*]

[a]*State Key Laboratory of Natural and Biomimetic Drugs, Peking University, Beijing 100191, China*
[b]*National Key Laboratory of Veterinary Public Health and Safety, College of Veterinary Medicine, China Agricultural University, Beijing 100193, China*
[c]*The Technology Center for Protein Sciences, Tsinghua University, Beijing 100084, China*

Received 29 July 2024; received in revised form 8 November 2024; accepted 12 December 2024

KEY WORDS

Natural product;
Marine fungus;
Antibiotic;
Bactericidal activity;
Peptaibol;
NRPS;
Phospholipid;
Phosphatidylglycerol

Abstract Antibiotic resistance is spreading at a faster rate than new antibiotic agents applied for clinical remedies. It is an urgent need to discover potential compounds to combat multidrug-resistant (MDR) bacteria. Marine fungi offer a promising avenue for mining antibiotic-like molecules with chemical diversity. To discover structurally novel and antibiotic metabolites, we screened the in-house marine fungus genome library and found a fungus *Stephanonectria keithii* LZD-10-1 containing a non-ribosomal peptide synthetase (NRPS) cluster with 18 modules to synthesize a new subfamily of peptaibols with effective eradication against MDR pathogens. Targeting isolation of the cultured fungus afforded six new peptaibols, which exhibit the ability to kill MDR bacteria by targeting bacterial membrane phospholipids, especially phosphatidylglycerol (PG), leading to the dysfunction of bacterial membranes. Furthermore, their efficacies against methicillin-resistant *Staphylococcus aureus* (MRSA) in both *Galleria mellonella* and mouse wound infection models were observed. This study underscores the significance of employing genome-guided approaches to identify untapped marine fungi as potential sources for novel antibiotic candidates with unique scaffolds.

*Corresponding authors.
E-mail addresses: zhuk@cau.edu.cn (Kui Zhu), whlin@bjmu.edu.cn (Wenhan Lin).
[†]These authors made equal contributions to this work.
Peer review under the responsibility of Chinese Pharmaceutical Association and Institute of Materia Medica, Chinese Academy of Medical Sciences.

https://doi.org/10.1016/j.apsb.2025.02.036

1. Introduction

Bacterial antimicrobial resistance (AMR) poses a grave threat to public health, with 1.27 million direct deaths and causing nearly five million deaths worldwide in 2019[1]. Multidrug-resistant (MDR) bacteria, especially those resisting last-resort antibiotics in clinical settings such as polymyxins[2] and tigecycline[3], have emerged as a particular concern. Regrettably, screening of new antibiotics has been hampered by the frequent rediscovery of compounds from terrestrial microorganisms[4,5]. Therefore, it is absolutely necessary to explore alternative sources for discovering novel antibiotics. Given the promising medicinal benefits, the vast and diverse marine microorganisms provide an attractive source of natural products[6-8]. The extreme marine niches under high-salinity and high-pressure force microbes to evolve sophisticated biosynthetic pathways with unique substrates for the production of structurally complex metabolites, which are used in hosts as chemical defense tools[9,10]. Actually, numerous marine-derived natural products including peptides[10], alkaloids[11], macrolides[12], and anthraquinones[13], have been found to exhibit antibiotic properties, providing alternative paradigms to search for new antibiotics. Compared to the increasing AMR from terrestrial origins and routine antibiotics, marine fungus-derived metabolites are characterized by their unique chemical structures with potential antibacterial activities, offering noticeable advantages[14,15].

Natural peptides synthesized by non-ribosomal peptide synthetases (NRPSs) are considered promising antibiotic candidates[16]. The modular nature of NRPSs with non-proteinogenic amino acids as substrates allows the production of diverse and novel peptide skeletons, that are not accessible through ribosome-dependent biosynthesis[17]. The structural diversity of such NRPS-derived peptides provides a rich resource as potential candidates with unique modes of action and offers the opportunity to identify multiple targets to combat MDR bacterial infections for the reduction of resistance development. For instance, daptomycin and polymyxins are the last-resort antibiotics to inhibit MDR Gram-positive and Gram-negative bacteria, respectively. Unfortunately, the devastating dissemination of resistance genes such as *mprF*[18] and *mcr-1*[2] has paralyzed their utilization, leading to the rising death of bacteria-associated infections. New NRPS peptides including clovibactin[19], macolacin[20], complestatin and corbomycin[21] are blooming, to potentially decelerate the emergence of MDR pathogens.

Among these naturally NRPS antibiotic peptides, peptaibols are a family of linear patterns with lengths ranging from five to 20 amino acids, and featuring a high proportion of non-proteinogenic Cα tetrasubstituted amino acids such as aminoisobutyric acid (Aib) or the more rare isovaline (Iva) with acylated *N*-terminal amino acid and *β*-amino alcohol for the C-terminus[22]. Due to the helical conformers caused by Aib or Iva residues, peptaibols act by destabilizing the lipid bilayer to create ion channels in membranes instead of a specific target[23], minimizing the possibility of resistance development[24]. Thus, peptaibols are promising molecules for the discovery of new antimicrobial drugs.

Recently, fungal genomics has unveiled a plethora of biosynthetic gene clusters (BGCs) that hold great probability for exploring antibiotics. Meanwhile, the incorporation of specific amino acids to the non-ribosomal peptides by a module can be empirically determined according to the A-domain substrate binding pocket[25], making it possible to find peptaibols by bioinformatics.

In this study, a new subfamily of peptaibols, SK-Ps, was isolated from a deep-sea fungus *Stephanonectria keithii* LZD-10-1[26,27] by BGC-guided screening. SK-Ps effectively kill multidrug-resistant bacteria by targeting bacterial membrane phospholipids, particularly phosphatidylglycerol (PG) and cardiolipin (CL), resulting in membranolytic activity. Upon binding to phospholipids, SK-Ps increase the membrane permeability, decrease proton motive force (PMF), and reduce ATP levels, leading to abnormal bacterial division and ultimately bacterial death. SK-Ps demonstrate promising antibacterial efficacy in two *in vivo* models, implying SK-Ps to be a new type of potential antibiotic candidate.

2. Results

2.1. Discovery of SK-Ps

To search for novel peptaibol-type antibiotics, we screened the in-house fungal genomes collected from the deep sea sediments and found a fungus *Stephanonectria keithii* LZD-10-1 containing 22 NRPS-like clusters accounting for 4.29% of the genome (predicted by antiSMASH 7.0[28], Supporting Information Table S1) with phenotypic inhibition against *S. aureus* ATCC 29213. Bioinformatics analysis showed that one NRPS gene cluster possesses 18 modules that encode Aib-containing peptides without matching known BGCs based on Stachelhaus codes (Supporting Information Table S2), indicating a high probability of triggering structurally novel peptaibol antibiotics.

Chemical annotation of the metabolite profile from the cultured strain using liquid chromatography-high resolution mass/mass (LC−HRMS/MS) data for molecular networking on the GNPS library (Supporting Information Fig. S1) uncovered a number of untapped linear peptaibols with molecular weights ranging from *m/z* 1767 to 1795. Targeting separation by chromatographic manipulation resulted in the isolation of six peptaibols namely SK-P1 to SK-P6 (**1**−**6**). Extensive analysis of the spectroscopic data established the linear sequences, while the configurations of amino acid residues were identified by both spectroscopic data in association with Marfey's methods (Supporting Information Figs. S13−S72, Supporting Information Tables S3−S11). SK-P1 to SK-P6 were structurally characterized by the presence of 18 amino acid residues with rarely methylated or free NH_2 for *N*-terminal instead of acylation, along with a high proportion of Aib and Iva residues (Fig. 1A and B). The sequence difference of **1**−**3** was attributed to residue-9 and residue-12, where Aib-9/Aib-12 for **1**, Aib-9/Iva-12 for **2**, and Iva-9/Iva-12 for **3** were characterized. Analogues **4**−**6** were identified as the *N*-demethylated homologues of **1**−**3**, respectively. Unlike the known peptaibols, SK-Ps are the peptaibols first discovered to contain an γ-aminobutyric acid (GABA) residue, demonstrating a new subtype of peptaibols. SK-Ps are slightly soluble in water

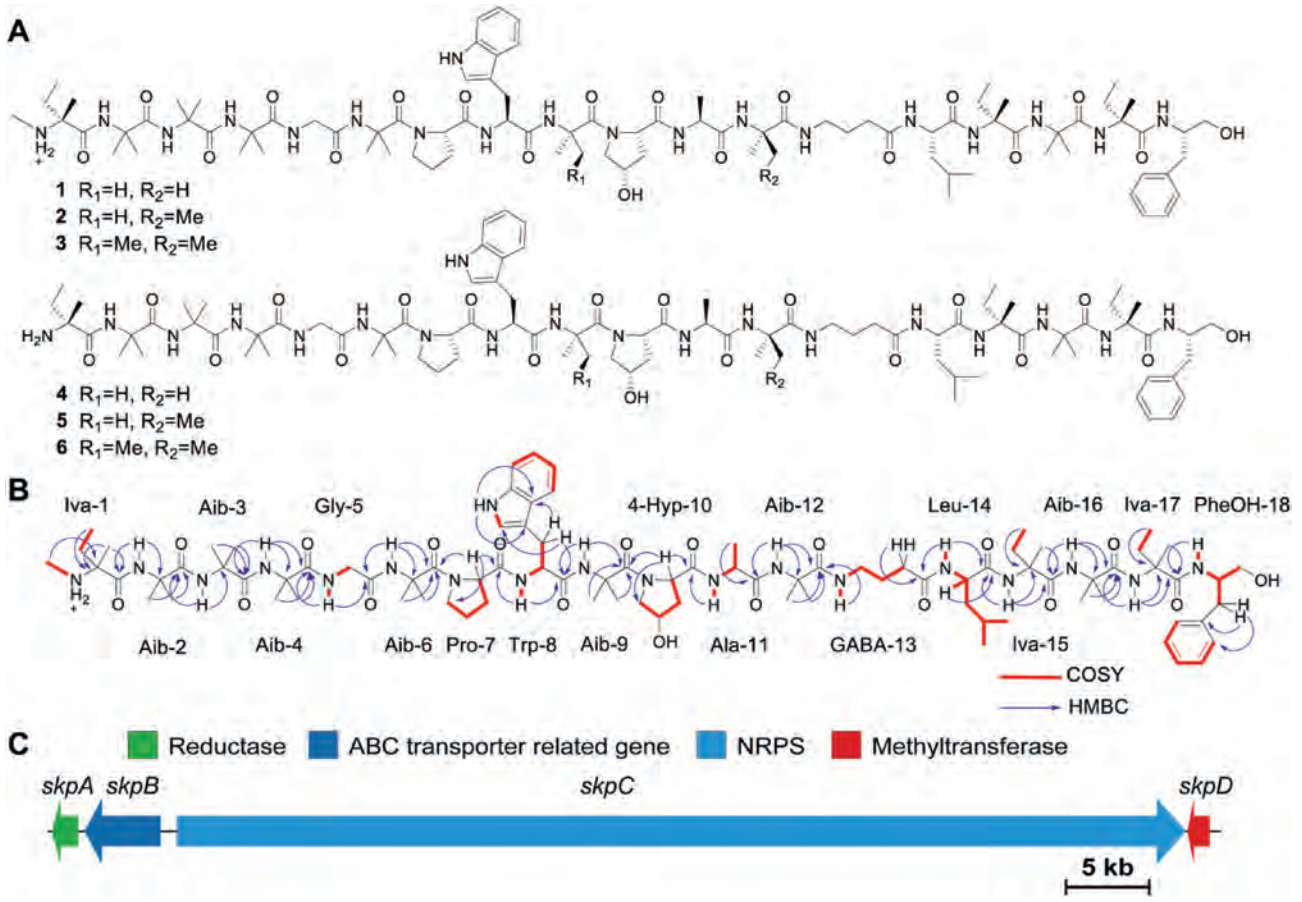

Figure 1 Structures of SK-Ps and biosynthesis gene cluster (*skp*). (A) Structures of 1−6. (B) Key COSY and HMBC correlations of SK-P1. (C) Biosynthetic gene cluster *skp* from fungus *S. keithii* LZD-10-1.

(approximately 130 μg/mL), but they exhibited potent inhibition against MDR Gram-positive bacteria with minimum inhibitory concentration (MIC) values comparable to the positive controls vancomycin and linezolid (Supporting Information Table S12, all strains used in this study are shown in Supporting Information Table S13). The similar antibiotic activities of SK-Ps (MIC value of 2.0 μg/mL) implied that the alternation of residue-9/residue-12 by Aib or Iva and the *N*-terminal with or without methyl group slightly affected the bioactivity. Apart from its resistance to pepsin and trypsin (Supporting Information Fig. S2A), SK-P1 maintained antibacterial activity under 70 °C or within a pH range from 5.2 to 10.2 for 1 h (Fig. S2B and S2C). However, highly acidic hydrolysis cleaved SK-Ps into fragments, such as SK-P2 is fragmented by acid to the moieties containing unit A (from residue-7 to residue-18) and unit B (from residue-10 to residue-18) (Supporting Information Fig. S3). Both fragments dramatically attenuated the activities with MIC values of more than 64 μg/mL (Table S12). These findings suggested the necessity to maintain the methylamine terminal or amine terminal for antibacterial properties, while the length and amino acid sequence of SK-Ps are also nonnegligible.

From a biogenetic point of view, only one NRPS gene cluster with 18 modules was recognized to possibly undertake the biosynthesis of SK-Ps (Table S1, cluster 8, Genbank: PP869428). The biosynthetic pathway for the generation of SK-Ps was postulated (Supporting Information Fig. S4), while the methyltransferase-catalyzed *N*-terminal methylation was likely located adjacent to the NRPS gene (Fig. 1C). The unique biosynthesis gene cluster, together with the new amino acid sequence and the presence of GABA led to the speculation of SK-Ps belonging to a new subfamily (SF) against known subfamilies of peptaibols[22], as show in Table 1[26,29-36]. Upon aligning the sequences using ClustalW V2.1 and constructing a phylogenetic tree, SK-Ps are recognized to be located at a new clade out of the conventional nine subfamilies (Fig. 2). Interestedly, SK-Ps reside near the clade of antibiotic agents microbacterins[26] and gichigamins[37]. Thus, SK-Ps are categorized into a new subfamily SF11. Collectively, these findings provided a new subtype of peptaibols with auspicious antibacterial activities.

2.2. *Inhibitory effects of SK-Ps against multidrug-resistant bacteria*

Subsequently, SK-P1 was selected as a candidate of SK-Ps to evaluate its antibacterial activities against a bacterium spectrum. First, SK-P1 showed inhibitory effects against a panel of Gram-positive pathogens with minimum inhibitory concentrations (MICs) ranging from 1 to 2 μg/mL (Table 2), including notorious methicillin-resistant *Staphylococcus aureus* (MRSA) and vancomycin-resistant *enterococci* (VRE), but it showed no effect against Gram-negative bacteria. In addition, the minimum bactericidal concentrations (MBCs) of SK-P1 showed 1- to 4- fold higher than MICs (Table 2), suggesting that SK-P1 is a bactericide. The time-killing curve demonstrated SK-P1 with an

Table 1 Amino acid sequence of representative peptaibols in different subfamilies.

SF	Peptaibol	1	2	3	4	5	6	7	8	9	10	11	12	13	14	15	16	17	18	19	20	Ref.
SF1	Alamethicin F-30	Aib	Pro	Aib	Ala	Aib	Ala	Gln	Aib	Val	Aib	Gly	Leu	Aib	Pro	Val	Aib	Aib	Glu	Gln	Phe	29
SF2	Emerimicin III	Phe	Aib	Aib	Aib	Val	Gly	Leu	Aib	Aib	Hyp	Gln	Iva	Hyp	Aib	Phe	–	–	–	–	–	29
SF3	Emerimicin II A	Trp	Ile	Gln	Aib	Ile	Thr	Aib	Leu	Aib	Hyp	Gln	Aib	Hyp	Aib	Pro	Phe	–	–	–	–	30
SF4	Trichobrachin A I	Aib	Asn	Leu	Leu	Aib	Pro	Leu	Aib	Aib	Pro	Leu	–	–	–	–	–	–	–	–	–	31
SF5	Trichogin A IV	Aib	Gly	Leu	Aib	Gly	Gly	Leu	Aib	Gly	Ile	Leu	–	–	–	–	–	–	–	–	–	32
SF6	Ampullosporin	Trp	Ala	Aib	Aib	Leu	Aib	Gln	Aib	Aib	Aib	Gln	Leu	Aib	Gln	Leu	–	–	–	–	–	33
SF7	LP237 F5	Aib	Pro	Tyr	Aib	Gln	Gln	Aib	EtNor	Gln	Ala	Leu	–	–	–	–	–	–	–	–	–	34
SF8	Clonostachin	Aib	Hyp	Leu	Iva	Hyp	Leu	Iva	Hyp	Aib	Iva	Aib	Hyp	Iva	Ile	–	–	–	–	–	–	35
SF9	Trichopolyn I	Ala	Aib	Aib	Ile	Ala	Aib	Aib	–	–	–	–	–	–	–	–	–	–	–	–	–	36
SF10	Microbacterins A	Aib	Pro	Ala	Aib	Aib	Phe	Iva	Pro	Ala	AHV	β-Ala	Leu	Iva	β-Ala	Leu	Aib	Aib	Leu	β-Ala	–	26
SF11	SK-P1	Iva	Aib	Aib	Aib	Gly	Aib	Pro	Trp	Aib	Hyp	Ala	Aib	GABA	Leu	Iva	Aib	Iva	Phe	–	–	This study

Note: Unique amino acids in peptaibols are shown in Bold. SF: subfamily; Iva: Isovaline; Aib: aminoisobutyric acid; Hyp: hydroxyproline; EtNor: ethylnorvaline; AHV: 3-amino-2-hydroxyvaline; GABA: γ-aminobutyric acid. "–" means not applicable.

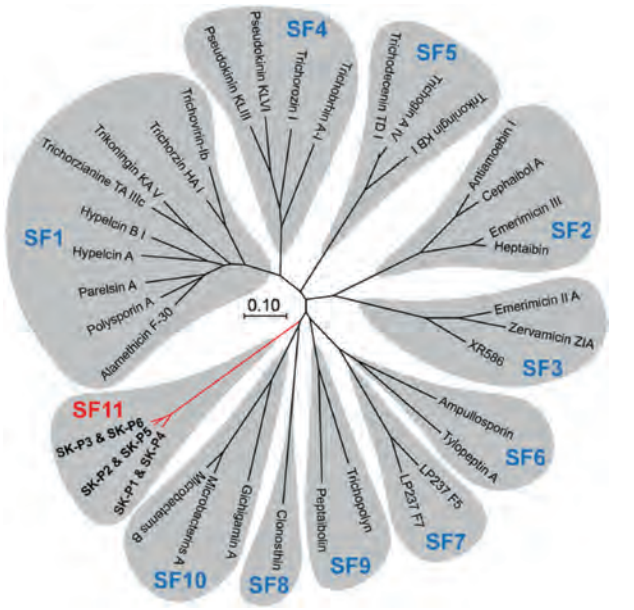

Figure 2 The phylogenetic tree of peptaibols based on the amino acid sequence. SK-Ps (SK−P1 to SK-P6) are involved in the clade SF11. The branch of SK-P1 overlaps with SK-P4, as does SK-P2 with SK-P5, and SK-P3 with SK-P6.

extremely rapid bactericidal activity, eliminating 10^6 CFU/mL bacteria within half an hour, significantly faster than vancomycin (Fig. 3A). Given that peptaibols can form pores in both mammalian and artificial lipid membranes to cause rapid leakage of intracellular contents[38,39], it is suggested that SK-P1 may also target bacterial membranes probably in the inner membrane. As in the cases of many antibiotics, SK-P1 exhibited no effectiveness against Gram-negative bacteria due to the presence of the non-permeable outer membrane, especially lipopolysaccharide (LPS)[40]. Therefore, we used colistin as an out-membrane disruptor[41] and found that SK-P1 and colistin synergistically inhibited MDR *Escherichia coli* B2, with the fractional inhibitory concentration index (FICI) of 0.14 (Fig. 3B). The inhibition of SK-P1 against LPS-deficient *Acinetobacter baumannii*[42,43] confirmed that SK-P1 acts on a common or shared target in

Table 2 Antibacterial activities of SK-P1 (μg/mL).

Strain (genotype)	SK-P1		Vancomycin
	MIC	MBC	MIC
S. aureus ATCC 29213	2	2	1
MRSA T144	1	2	1
MRSA 1530 (*cfr*)	1	4	1
S. equorum 2	2	2	2
S. simulans 4	1	4	1
S. lentus 12	2	2	1
B. subtilis ATCC 6051	2	2	0.5
E. faecalis 8-3 (*optrA*)	1	4	4
VRE CAU360 (*vanA*)	1	1	>128
VRE CAU369 (*vanA*)	1	1	>128
E. casselifavus 4w-9 (*optrA* + *cfr* + *vanC*)	1	2	8
C. perfringens C59-1	1	1	<0.25

All MIC assays were repeated at least in triplicate.

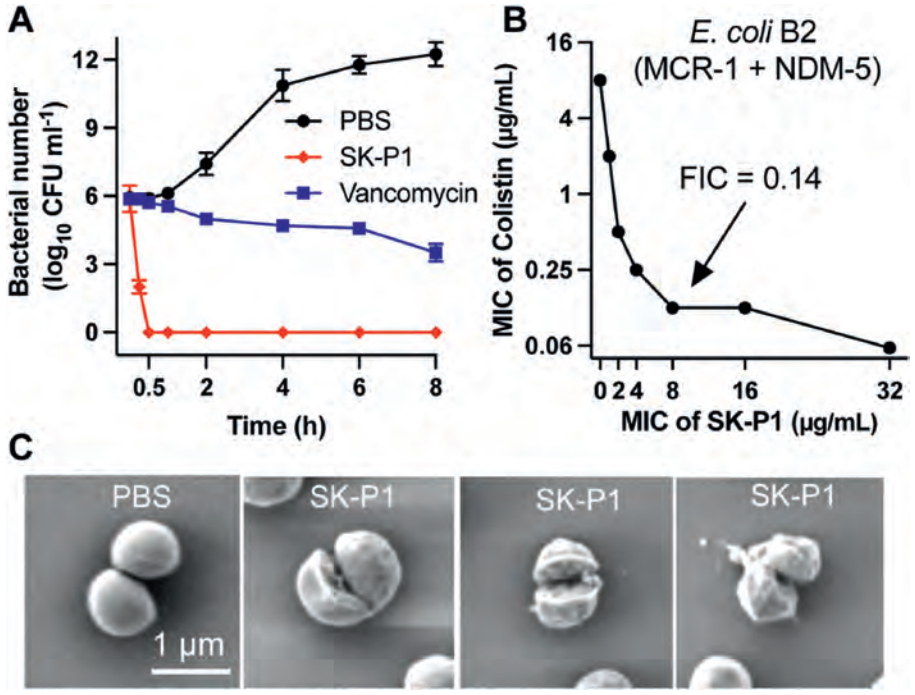

Figure 3 Bactericidal activity of SK-P1. (A) Time-dependent killing curves of SK-P1 (10 × MIC) against *S. aureus* ATCC 29213 at exponential phase. Vancomycin (10 × MIC) was used as a positive control. (B) Synergy of SK-P1 with colistin against MDR *E. coli* B2. (C) Morphological changes of *S. aureus* visualized by SEM. Data in (A) are obtained by three independent experiments and values are expressed in mean ± SD.

both Gram-positive and Gram-negative bacteria (Supporting Information Table S14). These results suggest that SK-Ps may target bacterial inner membrane or cytoplasmic components.

2.3. *Target of SK-Ps on bacterial phosphatidylglycerol*

To elucidate the mode of action of SK-Ps, we first detected the morphological changes of SK-P1-treated *S. aureus* ATCC 29213. Under the scanning electron microscope (SEM), obvious division abnormalities in *S. aureus* were observed (Fig. 3C), suggesting the incorrect positioning of the division site regulated by membrane phospholipids[44,45]. In light of classic peptaibol alamethicin forming ion channels in lipid membrane[38], we hypothesized that SK-P1 is directly bound to bacterial membrane phospholipids. Subsequently, three bacterial phospholipids including phosphatidylglycerol (PG), phosphatidylethanolamine (PE), cardiolipin (CL), and mammalian phospholipid phosphatidylcholine (PC) were exogenously added to detect the antibacterial activities of SK-P1 against *S. aureus*[46]. PG and CL completely abolished the activity of SK-P1 based on the disk diffusion method (Fig. 4A). The MIC value of SK-P1 against *S. aureus* increased dose-dependently in PG or CL solution (Fig. 4B), showing similar data as alamethicin in PG (against *S. aureus* ATCC 29213, MIC = 16 μg/mL, Supporting Information Fig. S5). Accordingly, the growth inhibition of SK-P1 against *S. aureus* was reversed in the presence of abundant PG (Supporting Information Fig. S6), implying that PG interrupted the interaction of SK-Ps with bacteria. To understand the mode of action, the PG liposomes were prepared by the thin-film hydration method (Supporting Information Fig. S7A and S7B). The dye leakage showed that SK-P1 exerted the disruption of lipid vesicles by around 60% of the dye released after incubation for 30 min (Fig. 4C), and the other SK-Ps and alamethicin showed similar results as SK-P1 (Fig. S7C), indicating the membranolytic activities of SK-Ps.

To investigate whether SK-P1 directly bonds to PG, the isothermal titration calorimetry (ITC) analysis was performed. The affinity (K_D) between PG and SK-P1 was 3.12×10^{-7} mol/L, with the stoichiometric ratio of PG to SK-P1 at 0.77 (Fig. 4D), meaning that SK-Ps could strongly bind to PG. It is noteworthy that the replacement of Aib in SK-P1 to Iva in SK-P2 did not affect the affinity to PG ($K_D = 4.39 \times 10^{-7}$ mol/L, Supporting Information Fig. S8A and S8B), but SK-P5 with demethylated *N*-terminal significantly weakened the affinity with approximate 20-fold ($K_D = 7.7 \times 10^{-6}$ mol/L, Fig. S8A and S8C). To decipher the binding kinetics between SK-P1 and PG, we calculated the Gibbs free energy based on ITC analysis. Compared to the molar binding entropy ($-T\Delta S = -8.29$ kJ/mol), the molar binding enthalpy ($\Delta H = -28.9$ kJ/mol) dominates the binding, indicating that SK-P1 mainly binds to PG with hydrogen bond. Therefore, we separately co-incubated SK-Ps with PG for hydrogen nuclear magnetic resonance (^{1}H NMR) analysis. In comparison with the ^{1}H NMR data of SK-P2, the intensity of terminal $MeNH_2$ signals in SK-P2/PG was decreased, whereas the terminal NH_2 signals in demethylated SK-P5 were unchanged (Supporting Information Fig. S9). Given the reduced affinity between SK-P5 and PG, the terminal $MeNH_2$ cation is crucial for binding. Considering the similar MIC values (Table S12) and time-dependent killing curves (Supporting Information Fig. S10) of SK-P2 and SK-P5, we speculated that PG may not be the sole antibacterial target for SK-Ps. It is conceivable that SK-Ps initially anchor to the bacterial cell membrane and subsequently interact with unidentified secondary targets, thereby exerting further bactericidal effects. These interactions with alternative targets may be independent of N-terminal methylation in SK-Ps.

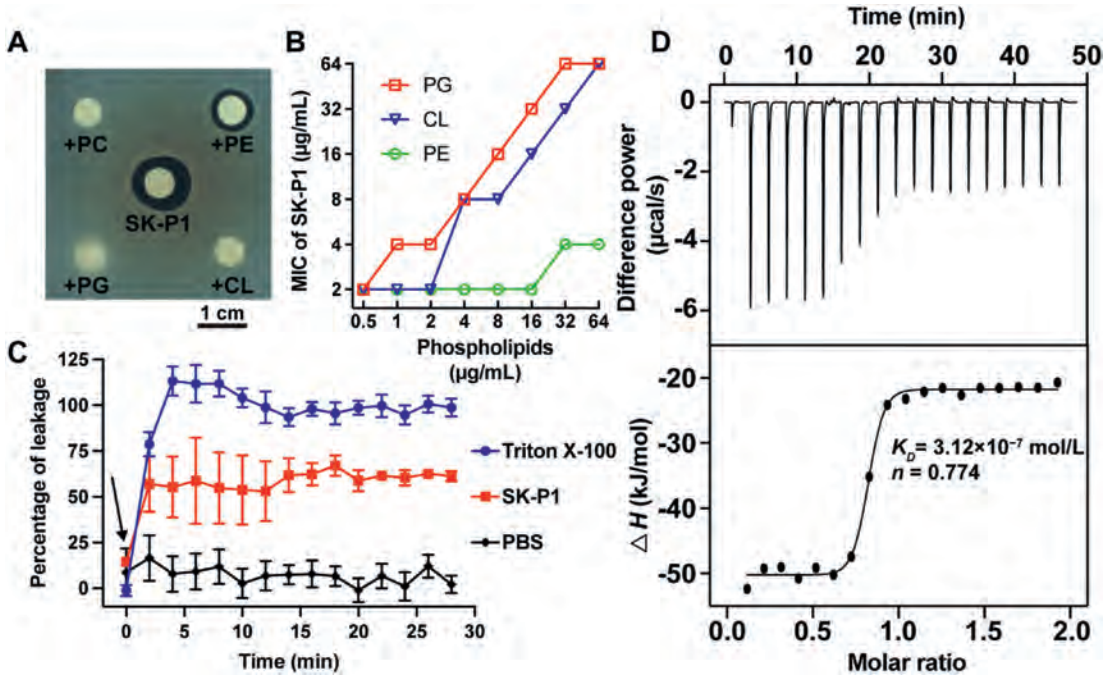

Figure 4 Membranolytic activity of SK-P1 by targeting bacterial membrane phospholipids. (A) Inhibition zones of the mixtures of SK-P1 (2 μg) with PC, PE, PG, or CL (5 μg) against *S. aureus*. (B) Dose-dependent increase of SK-P1 against *S. aureus* in the presence of membrane phospholipids. (C) Leakage of 5-carboxyfluorescein dye from PG liposomes treated with SK-P1. The arrow means compounds added at this time. (D) ITC analysis of the interaction between SK-P1 and PG. Thermodynamic parameters were calculated, including the equilibrium dissociation constant (K_D), number of binding sites (n), molar binding enthalpy (ΔH) and molar binding entropy (ΔS). Data in (C) are obtained by three independent experiments and values are expressed in mean ± SD.

PG is a common membrane phospholipid in both Gram-positive and Gram-negative bacteria. In certain bacterial species such as *S. aureus*, PG constitutes up to approximately 80% of membrane phospholipids[47]. Antibacterial NRPS peptides and ribosomally synthesized cathelicidin have been demonstrated to effectively target bacterial membrane phospholipids such as PG.[48,49,60] For instance, daptomycin binds to PG ($K_D = 3.1 \times 10^{-6}$ mol/L) forming a tricomplex with undecaprenyl-coupled cell envelope precursors, resulting in the interruption of cell wall synthesis[51,52]. Moreover, the high affinity between PG and linear peptide SLAP-S25 ($K_D = 5.76 \times 10^{-7}$ mol/L) exhibits a broad spectrum of antibacterial potential[46]. The SK-Ps binding to PG may serve as a common mechanism for peptaibols against bacterial pathogens.

2.4. *Induction of SK-Ps on bacterial membrane dysfunction*

To understand the effect of SK-Ps against bacteria after the binding of SK-Ps to PG, we focused on the subsequent dysfunction of the membrane. First, we assessed the impact of SK-Ps on membrane permeability in *S. aureus*. SK-P1 rapidly disrupted membrane integrity, leading to the binding of propidium iodide to bacterial nucleic acid. Interestingly, SK-P1 rapidly increased the membrane permeability, showing faster than the positive control nisin (Fig. 5A), an antibiotic agent widely used for pore formation in bacterial membranes. This result agreed with the observation that SK-Ps are rapid bactericides and target bacterial phospholipids. Consequently, the disruption of membrane integrity always results in the dissipation of proton motive force (PMF)[53,54], which is composed of membrane potential ($\Delta\psi$) and ΔpH. Hence, we evaluated the effect of SK-P1 on $\Delta\psi$ and ΔpH using fluorescent probes $DiSC_3(5)$ and BCECF-AM, and found that SK-P1 caused the dissipation of both $\Delta\psi$ and ΔpH (Fig. 5B and C). Disrupted membrane homeostasis promotes the accumulation of reactive oxygen species (ROS) and suspension of energy production, causing bacterial death[55]. However, we do not observe any ROS accumulation in SK-P1-treated *S. aureus* (Supporting Information Fig. S11). Nevertheless, we deduced that SK-P1 blocked the generation of adenosine triphosphate (ATP) by PMF, as evident from a dose-dependent decrease of total ATP levels in *S. aureus* after the treatment of SK-P1 for 1 h (Fig. 5D). Correspondingly, the extracellular ATP levels increased accompanying the disrupted bacterial membrane integrity. Altogether, the binding of SK-Ps to PG disrupts membrane homeostasis, triggering the subsequent membrane dysfunction, abnormal replication, and ultimately causing bacterial death (Fig. 5E).

2.5. *In vivo efficacy of SK-Ps*

It is noted that many reported antibacterial peptides are ineffective *in vivo* due to the presence of serum and physiological salts[56]. In this study, SK-P1 maintained antimicrobial activity in serum and cationic environments (Supporting Information Table S15), and showed no hemolysis activity at 100 μg/mL. However, SK-P1 exhibited cytotoxicity against mammalian cells (Supporting Information Fig. S12), which may be attributed to its target on PC in mammalian cells. To detect the efficacy of SK-Ps *in vivo*, a simplified insect *G. mellonella* infection model[57] and a mouse wound infection model were established (Fig. 6A). Initially, *G. mellonella* larvae were infected with a lethal dose of MRSA T144 to create a model with resistant bacterial infection. Compared to

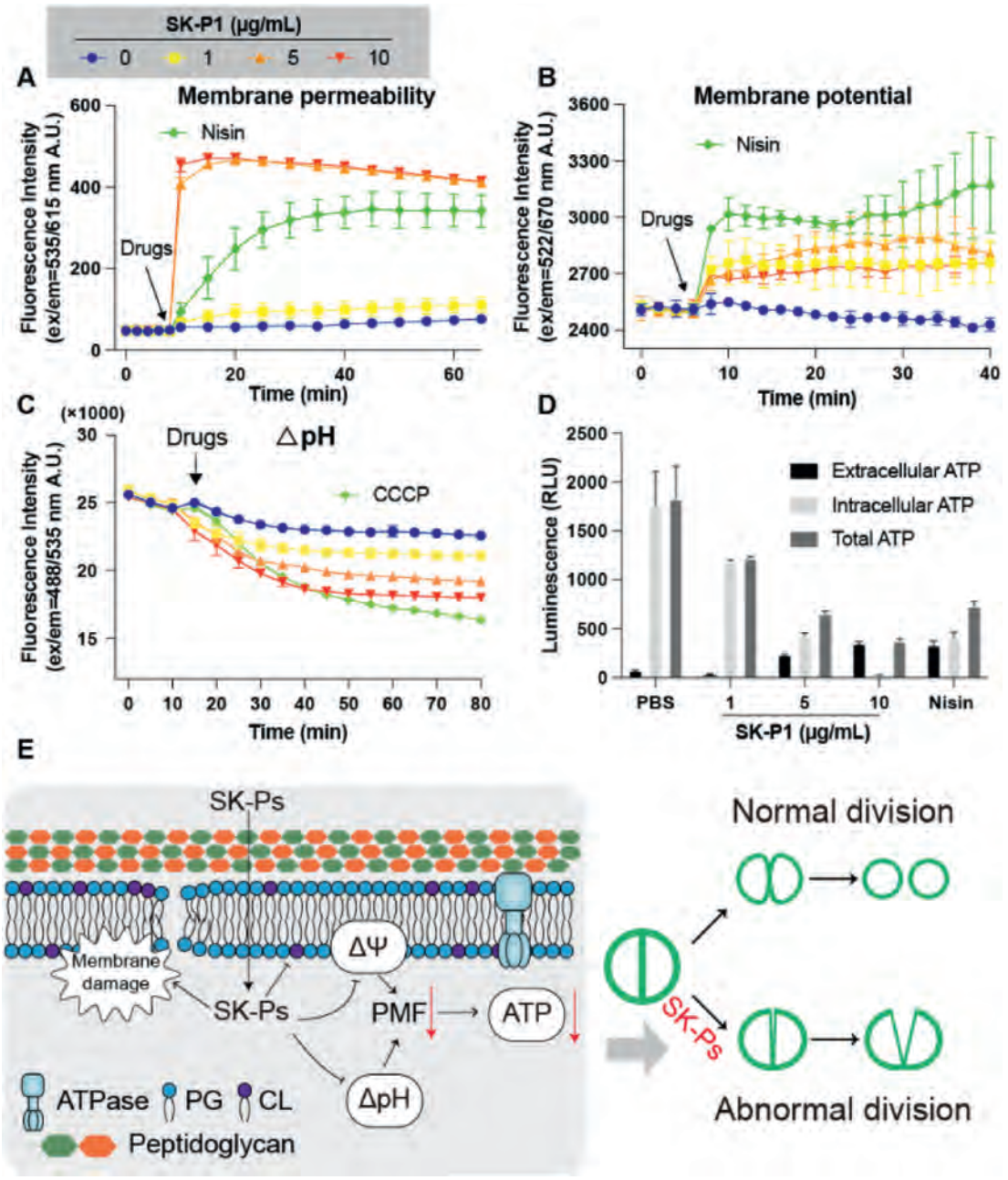

Figure 5 SK-P1 causes bacterial membrane dysfunction. *S. aureus* ATCC 29213 treated with SK-P1 results in (A) an increase of membrane permeability, dissipation of (B) membrane potential and (C) ΔpH, and (D) a decrease of total ATP. (E) Tentative scheme of the mode of action of SK-Ps against *S. aureus*. Data are obtained by three independent experiments and values are expressed in mean ± SD.

the PBS control, SK-P1 rescued the survival of insects significantly (Fig. 6B), and markedly reduced the bacterial loads within the larvae (Fig. 6C). These findings suggested that SK-P1 effectively protected *G. mellonella* larvae from MRSA infection. In addition, SK-P1 exhibited the ability to promote wound healing in the MRSA wound infection model (Fig. 6D and E) with decreased bacterial loads in the wounds on the 12th day post-infection (Fig. 6F), and the data were comparable to the group treated with vancomycin. Notably, SK-P1 also showed comparable anti-inflammatory activities to vancomycin, as evident from the similar inhibitory effects of both SK-P1 and vancomycin against TNF-α and IL-6 in the wounds (Fig. 6G).

3. Discussion

The findings above suggested that SK-P1 is a potential agent for the treatment of MDR infections *in vivo*, and indicated that SK-P1 was suitable for the treatment of skin infection by MRSA bacteria. Due to the cytotoxicity of SK-Ps toward mammalian cells, future extension of SK-P type peptaibols by structural modification to mitigate cytotoxic effect is required if it is applied for oral taking or injection. The potent antibacterial activities of SK-Ps are attributed to their selective interaction with phospholipids, as evidenced by varying antibacterial activity upon the addition of different phospholipids (Fig. 4). This selectivity is likely

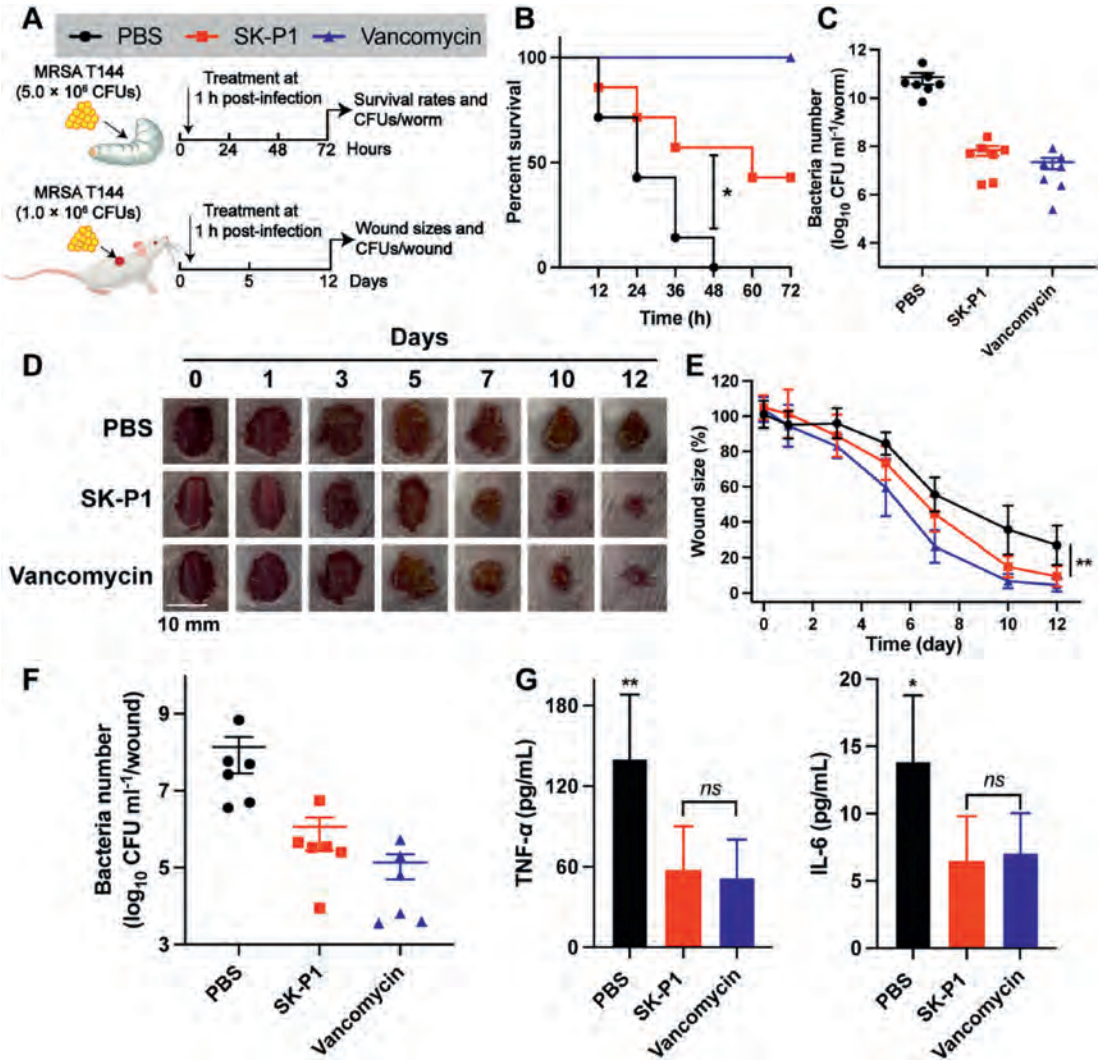

Figure 6 Efficacy of SK-P1 in *G. mellonella* and mouse models. (A) Scheme of the experimental protocol for the *G. mellonella* and mouse skin wound infection models. (B) Survival rates of *G. mellonella* larva infected with MRSA T144 (5.0×10^6 CFUs) in the presence of SK-P1 ($n = 7$). Vancomycin was used as a positive control. (C) SK-P1 (10 mg/kg) and vancomycin (10 mg/kg) both decreased bacterial loads in *G. mellonella*. (D) Representative photographs of wound sizes in the mouse skin wound infection model treated with SK-P1 (10 mg/kg) after infection of MRSA T144 (1.0×10^6 CFUs) on different days ($n = 6$). Scale bar = 10 mm. (E) Increased wound closure of mouse in 12 days treated with SK-P1. (F) Bacterial loads in the wound on the 12th day post-infection ($n = 6$). (G) The TNF-α (left) and IL-6 (right) expression levels decreased after SK-P1 treatment. Data are representative of seven independent experiments in (B) and (C), and six independent experiments in (E), (F), and (G). Values are expressed in mean ± SEM in (C) and (F), and mean ± SD in (E) and (G). *$P < 0.05$; **$P < 0.01$; *ns*: not significant, $P > 0.05$. *P*-values in (B) were determined by the log-rank (Mantel−Cox) test and in (E) and (G) were determined by unpaired *t*-tests, using PRISM 9.

correlated to the headgroups of the phospholipids. To address this, further mechanism investigation of specific binding between SK-Ps and phospholipids may help to find potent antibacterial candidates with low cytotoxicity. Structure modification of SK-Ps is expected to specifically target PG for enhancement of antimicrobial activity, whereas analogues targeting PC are unfavorable due to the correlation to cytotoxicity. In addition to the biogenetic manipulation, solid-phase peptide synthesis (SPPS) provides an alternative strategy for scale-up preparation of lead compounds, and chemical diversity for SAR discussion is helpful to improve antibacterial leads with potent activity and low toxicity.

4. Conclusions

In summary, our work highlights the importance of employing genome-guided approaches to identify bioactive natural products with novel scaffolds in marine fungi. Moreover, the newly identified subfamily of peptaibols, SK-Ps, exhibits the ability to target bacterial membrane phospholipids, specifically PG, leading to disruption of bacterial membrane functionality and ultimately bacterial death. The rapid bactericidal activity of SK-Ps allows for the swift elimination of infecting bacteria *in vitro* and *in vivo*, making it a potential antibiotic candidate.

5. Experimental section

5.1. General methods

Optical rotations were measured on a Rudolph Research Autopol IV automatic polarimeter. NMR data were obtained on Bruker Avance (Karlsruhe, Germany) 800 MHz and 600 MHz spectrometers equipped with CryoProbe (800 and 600 MHz for ^{1}H, 200 and 150 MHz for ^{13}C) with broadband and triple resonance probes. Electrospray-ionization mass spectrometry, MS^n ($n = 2$ or 3), and single-cell mass data were collected on a Thermo Q Orbitrap mass spectrometer (Thermo Fisher Scientific Inc., MA, USA). TLC detection was carried out using precoated silica gel plates (Yantai Chem. Ind., Yantai, China). Column chromatography was performed on Silica gel (200−300 mesh, Qingdao Marine Chemical Plant, Qingdao, China). ODS (50 μm) was provided by YMC Co. (Kyoto, Japan), and Sephadex-LH20 (18−110 μm) was obtained from Pharmacia Co. (Peapack, NJ, USA). High-performance liquid chromatography (HPLC) was performed on Waters UPLC equipped with a UV detector (Waters, Milford, USA). All-tech semi-preparative HPLC system equipped with the Model 201 UV detector and Waters SunFire 5 μm C18 column (110 Å, 250 × 10.0 mm) was used for compound purification with a flow rate of 2 mL/min. The experimental ECD spectrum was measured with a Jasco-1500 circular dichroism spectrometer. All solvents were of ACS grade or better.

5.2. Fungal strain

Fungus *Stephanonectria keithii* LZD-10-1 was isolated from a gorgonian *Peseudopterogorgia* sp. (LZD-10) collected from the South China Sea in May 2015. The strain was identified by comparing the morphological characteristics and analysis of the ITS region of the rDNA sequence with those of standard records (GeneBank MT670423). The strain LZD-10-1 was deposited at the State Key Laboratory of Natural and Biomimetic Drugs, Peking University.

5.3. Bioinformatic analysis

The NRPS/NRPS-like clusters and NRPS A-domain were analyzed using the online antiSMASH v.7.0 (fungal version) web tool to identify the fungal BGC and the amino acids that make up its A-domain substrate binding pocket (amino acids 235, 236, 239, 278, 299, 301, 322, 330, 331 and 517).

5.4. Fermentation and extraction

Fungal fermentation was carried out in 30 Fernbach flasks (500 mL), each containing 80 g of rice. Distilled artificial seawater (100 mL) was added to each flask, and the contents were soaked overnight before autoclaving at 15 psi for 30 min. After cooling to room temperature, each flask was inoculated with 5.0 mL of the mycelium and incubated at 25 °C for 50 days. The fermented material was extracted successively with EtOAc (3 × 400 mL). After evaporation under vacuum, the EtOAc extract (9.1 g) was obtained.

5.5. SPE fractionation

Ion exchangeable resin solid phase extraction (SPE) was carried out using Waters OASIS SPE columns. The crude extract of LZD-10-1 (10.2 mg) was dissolved in 1 mL MeOH and centrifugated for 2 min. The supernatant was loaded on the Waters OASIS HLB column (5 mL) and washed with 10 mL MeOH. After evaporation under vacuum, the extract was redissolved in 1 mL MeOH and centrifuged for 2 min to obtain a standard sample (supernatant), which was then loaded on Water OASIS WCX column (5 mL) and eluted with a mobile phase of 2 mL 5% ammonia, 4 mL MeOH and 4 mL 2% HCOOH sequentially. The 2% HCOOH/MeOH solution was evaporated under a vacuum, the extract was dissolved in 1 mL MeOH to obtain the WCX sample (strong alkaline compounds). WCX sample was then loaded on Water OASIS MCX column (5 mL) and eluted with 2 mL 2% formic acid, 4 mL MeOH, and 4 mL 5% NH_3/MeOH sequentially. The fraction of 5% NH_3/MeOH eluent mainly contained weak alkaline compounds (MCX sample). Following the same protocol, the MeOH eluent was then loaded on the Water OASIS WAX column (5 mL) and eluted with 2 mL 2% formic acid, 4 mL MeOH, and 4 mL 5% NH_3/MeOH sequentially. Evaporation of the 5% NH_3/MeOH eluent under vacuum obtained the WAX extract (strong acidic compounds). The MeOH eluent was loaded on the Water OASIS MAX column (5 mL) and eluted with 2 mL 5% NH_3 solution, 4 mL MeOH, and 4 mL 2% NH_3/MeOH sequentially. The 2% HCOOH/MeOH eluent was evaporated under a vacuum and redissolved in 1 mL MeOH to obtain the MAX sample (weak acidic compounds). The MeOH eluent was evaporated under a vacuum to obtain neutral compounds. All the SPE fractionations were collected to test the MIC values against *S. aureus* ATCC 29213.

5.6. Analysis of LC-HRMS data

The metabolite profiles of SPE fractions were analyzed by UPLC (Thermo), using an analytical chromatographic BEH C_{18} column (2.1 × 100 mm, 1.7 μm) coupled to a mass spectrometer (Thermo Q Orbitrap) with electrospray ionization (ESI). Samples were solubilized in MeOH and filtered with PVDF filters (0.22 μm). The separation process was performed through a gradient system using water with 0.1% HCOOH as solvent A and MeOH as solvent B (injection volume of 10 μL and flow rate of 0.3 mL/min). HRMS instrument with an electrospray ionization (ESI) probe was tuned and calibrated in ESI + using positive calibration solutions once a week. MS parameters were set as follows: spray voltage (3.8 kV), capillary temperature (325 °C), probe heater temperature (350 °C), and S-Lens (60 V). HRMS data were acquired in full scan (FS)/data-dependent fragmentation acquisition (dd-MS2) mode. In FS, mass resolution, AGC target, and maximum IT were set at 70,000 FWHM, 3.0×10^6, and 100 ms, respectively; the scan range was set at *m/z* 100−2500. In dd-MS2, mass resolution (17,500 FWHM), AGC target (1.0×10^5), maximum IT (30 ms), Top N (5), and stepped normalized collision energy (NCE) (10%, 30% and 50%) were set.

5.7. Molecular networking

The data obtained by LC−MS/MS were converted into mzXML format directly from Bruker DataAnalysis 4.2. The molecular networking was generated using GNPS (http://gnps.ucsd.edu) with the following parameters: parent mass tolerance of 2.0 Da, Ms/Ms fragment ion tolerance of 0.5 Da, cosine score of 0.7, and minimum matched peaks of 6. The data were subsequently visualized using the Cytoscape 3.9.1 software.

5.8. Isolation of SK-Ps (1−6)

The EtOAc extract (9.1 g) was subjected to a vacuum liquid chromatography (silica gel, 200−300 mesh) with petroleum ether/acetone (from 20:1 to 0:1, gradient) as an eluent to obtain seven fractions (F1 to F7). ^{1}H NMR and DAD−UPLC/MS analysis of each fraction was carried out, the result indicated that fraction F6 (petroleum ether/acetone 1:1) contained peptide analogues (D_2O changeable proton signals of NH in ^{1}H NMR, *m/z* > 1000 Da in UPLC/MS). F6 (732.4 mg) was further subjected to an ODS column (450 × 48 mm, 50 μm) eluting with gradient MeOH/H_2O (10:90 to 100:0) to afford ten fractions (F6-1-F6-10). F6-8 (MeOH/H_2O 80:20, 345.1 mg) was further purified by semi-preparative HPLC eluting with MeCN/H_2O (74: 26, *v/v*) to give **1** (74.1 mg), **2** (103.4 mg), **3** (8.6 mg), **4** (11.2 mg), **5** (7.9 mg), **6** (1.4 mg).

SK-P1 (**1**): Colorless powder, $[\alpha]_D^{20}$ 50 (*c* 0.2, MeOH); IR ν_{max} (KBr) 3296, 2984, 2939, 1651, 1541, 1458, 1386 cm^{-1}; ^{1}H- and ^{13}C-NMR data, see Table S3. HRESIMS *m/z* 1781.0676 $[M]^+$ (Calcd for $C_{89}H_{142}N_{19}O_{19}$, 1781.07239).

SK-P2 (**2**): Colorless powder, $[\alpha]_D^{20}$ 46 (*c* 0.2, MeOH); IR ν_{max} (KBr) 3296, 2984, 2940, 1651, 1543, 1458, 1387 cm^{-1}; ^{1}H- and ^{13}C-NMR data, see Table S4. HRESIMS *m/z* 1795.0836 $[M]^+$ (Calcd for $C_{90}H_{144}N_{19}O_{19}$, 1795.08804).

SK-P3 (**3**): Colorless powder, $[\alpha]_D^{20}$ 50 (*c* 0.2, MeOH); ^{1}H- and ^{13}C-NMR data, see Table S5. HRESIMS *m/z* 1809.09448 $[M]^+$ (Calcd for $C_{91}H_{146}N_{19}O_{19}$, 1809.10369).

SK-P4 (**4**): Colorless powder, $[\alpha]_D^{20}$ 43 (*c* 0.2, MeOH); ^{1}H- and ^{13}C-NMR data, see Table S6. HRESIMS *m/z* 1767.04944 $[M+H]^+$ (Calcd for $C_{88}H_{140}N_{19}O_{19}$, 1767.05674).

SK-P5 (**5**): Colorless powder, $[\alpha]_D^{20}$ 46 (*c* 0.2, MeOH); ^{1}H- and ^{13}C-NMR data, see Table S7. HRESIMS *m/z* 1781.06299 $[M+H]^+$ (Calcd for $C_{89}H_{142}N_{19}O_{19}$, 1781.07239).

SK-P6 (**6**): Colorless powder, $[\alpha]_D^{20}$ 50 (*c* 0.2, MeOH); ^{1}H- and ^{13}C-NMR data, see Table S8. HRESIMS *m/z* 1795.07971 $[M+H]^+$ (Calcd for $C_{90}H_{144}N_{19}O_{19}$, 1795.08804).

5.9. Structural elucidation of SK-Ps

SK-P1(**1**) was determined to have a molecular formula of $C_{89}H_{142}N_{19}O_{19}$ by the HRESIMS (*m/z* 1781.0676 $[M]^+$) and NMR data. The ^{1}H NMR spectrum exhibited 18 D_2O changeable protons among δ_H 7−9 ppm for amide resonances, five α-H (δ_H 4−5), and numerous protons in the alkyl region involving 17 methyl singlets. The ^{13}C NMR data afforded 17 carbonyl carbons (δ_C 165−176) and the resonances among δ_C 50−70 and δ_C 5−40 (Table S3). These data in association with the MS/MS data suggested SK-P1 to be a peptaibol derivative. Interpretation of the HMBC and COSY data established 18 amino acid residues, including a Trp (tryptophan), a Gly(glycine), an Ala (alanine), a Pro (proline), a Leu (leucine), a 3-carboxypropylamine, a 4-hydroxylproline, three Iva (isovaline), seven Aib (amino-isobutyric acid), as well as a phenylalaninol. A phenylalaninol for C-terminal was identified by the COSY correlations between NH (δ_H 7.06, d, J = 7.2 Hz)/α-H (δ_H 3.85, m), from α-H to β-H_2 (δ_H 2.10, 1.70, m) and γ-H_2 (δ_H 3.35, δ_H 3.27, m), between γ-H_2/OH (δ_H 3.85), in addition to the presence of five aromatic protons for a mono-substituted phenyl group and the HMBC correlations from β-H_2 to aromatic carbons δ_C 139.4 and δ_C 129.1. The NMR resonances of three Iva residues were characterized by the presence of methyl triplets at δ_H 0.83 (t, J = 7.5 Hz), 0.77 (t, J = 7.5 Hz), and 0.77 (t, J = 7.5 Hz), and the HMBC interactions from the methyl protons to the quaternary Cα at δ_C 64.9, 58.9, and 59.3, respectively. A 4-hydroxylproline was recognized by Cγ at δ_C 69.1 and the COSY correlations from Hγ (δ_H 4.18, m) to methylene protons (δ_H 2.10, 1.71 and δ_H 3.61, 3.36), along with the HMBC correlation from Hγ to Cα (δ_C 61.3). The NOE correlation between Hα (δ_H 4.34) and Hγ suggested both protons in the same face. For the *N*-terminal, a methyl triplet at δ_H 2.45 (t, J = 5.0 Hz) showed the COSY correlation with D_2O changeable NH_2 (δ_H 8.93 and 8.84) and the HMBC correlation with Cα (δ_C 64.9) of an Iva, demonstrating a *N*-methylated Iva. The sequential assignment was carried out by the NOE interactions from NH to Hα of adjacent residue, in association with the HMBC correlations from the carbonyl carbons to Hα of the next residues. Thus, a sequence of NMe-Iva-Aib-Aib-Aib-Gly-Aib-Pro-Trp-Aib-Hyp-Ala-Aib-GABA-Leu-Iva-Aib-Iva-Phe-OH was established. The ESI−MS/MS data provided a molecular ion at *m/z* 1781.0676 $[M]^+$ following daughter ions at *m/z* 1119, 751, and 511 for the fragments supported the sequence assignment. The absolute configuration of **1** was determined by the acidic hydrolysis of **1** and subsequent derivatization according to Marfey's method. Comparison of the resulting derivatives with those of appropriate standard amino acids using UPLC−MS techniques indicated L-form for Ala, Trp, Leu, and D-form for Pro and *cis*-Hyp. The absolute configuration of Iva residue can be determined based on the chemical shifts of its ethyl group[58]. The chemical shifts of γ-H_3 (δ_H 0.83 for Iva-1, δ_H 0.77 for Iva-15, δ_H 0.51 for Iva-17, <0.89 ppm), and β-CH_2 (δ_C 28.5 for Iva-1, δ_C 28.2 for Iva-15, δ_C 29.7 for Iva-17, <30 ppm), and $\Delta\delta_{\beta Hb\text{-}\beta Ha}$ (0.06 for Iva-1, 0.24 for Iva-15, 0.30 for Iva-17, Iva-17 and Iva-17 > 0.20 ppm) (Table S11) were in agreement with the *R*-configuration for Iva residue. Acidic hydrolysis of compound **1** and semi-preparative HPLC purification resulted in the isolation of phenylalaninol residue. A comparison of its optical values with those of the standard confirmed the L-configuration of phenylalaninol moiety.

The structures of SK-P2 to SK-P6 (**2**−**6**) were determined on the basis of 1D and 2D NMR data in association with the MS/MS fragmentation and Marfey's method.

5.10. Marfey's analysis

SK-P1 (0.2 mg) was dissolved in 6N HCl (0.5 mL) within a vial. The mixture was heated at 110 °C for 24 h and then evaporated under vacuum. The hydrolyzed products were reacted with 1% Marfey's reagent in acetone (50 μL) by adding 25 μL H_2O and 10 μL 1 mol/L $NaHCO_3$ to stir for 1 h at 40 °C and then quenched by adding five μL 2N HCl. The MeOH solution of products was analyzed by the UPLC (BEH column) with 10%−70% MeOH−H_2O as a mobile phase monitored under 340 nm. Authentic amino acids (each 0.2 mg) were reacted with 1% Marfey's reagent (100 μL) in acetone under 50 μL H_2O and 20 μL 1 mol/L $NaHCO_3$ for 1 h at 40 °C. The UPLC detection was performed by the same protocol as for the hydrolyzed products of SK-P1.

5.11. Hydrolysis of SK-P2 (2)

SK-P2 (**2**, 10 mg) was dissolved in five mL 12 N HCl and stayed overnight at room temperature. The resulting mixture was dried under N_2. The residue (11 mg) was purified by semipreparative HPLC (eluted with 30%−50% MeCN in 0.05% formic acid) to yield unit A (1.1 mg) and unit B (0.9 mg) as the main products.

Unit A: Colorless powder, $[\alpha]_D^{20}$ 30 (*c* 0.2, MeOH); ^{1}H- and ^{13}C-NMR data, see Table S9. HRESIMS *m/z* 1284.76416 $[M]^+$ (Calcd for $C_{66}H_{102}N_{13}O_{13}$, 1284.77146).

Unit B: Colorless powder, $[\alpha]_D^{20}$ −10 (*c* 0.2, MeOH); ^{1}H- and ^{13}C-NMR data, see Table S10. HRESIMS *m/z* 916.58307 $[M]^+$ (Calcd for $C_{46}H_{78}N_9O_{10,}$ 916.58662).

5.12. Antibacterial test

Minimum inhibitory concentrations (MICs) of SK-Ps and different antibiotics were determined by the standard broth microdilution method according to the Clinical & Laboratory Standards Institute (CLSI) M100 guideline. Briefly, SK-Ps and antibiotics were 2-fold serial diluted in Mueller−Hinton broth (MHB, CM901, Beijing Land Bridge Technology Co., LTD., Beijing, China) in a clear UV-sterilized 96-well microtiter plate (Corning Inc., New York, USA) and mixed with equal volumes of bacterial suspensions in MHB containing approximately 1×10^6 colony-forming units (CFUs)/mL. Vancomycin/linezolid was used as the positive control against Gram-positive bacteria, colistin was used as the positive control against Gram-negative bacteria. After 16−20 h incubation at 37 °C, the MIC values were defined as the lowest concentrations of SK-Ps and antibiotics with no visible growth of bacteria. The tested bacterial strains are listed in Table S13.

5.13. Time-dependent killing curve

An overnight cultured *S. aureus* ATCC 29213 was diluted to 1:10,000 in MHB and incubated at 37 °C with shaking at 200 rpm for 2 h to obtain the bacteria in the exponential phase. Then bacteria were adjusted to a concentration of approximately 1×10^6 CFU/mL and challenged with antibiotics or SK-P1 at 10 × MIC in culture tubes at 37 °C with shaking at 200 rpm. At every point in time, 10-fold serially diluted suspensions were plated on TSA plates and incubated overnight at 37 °C for enumeration of bacterial colonies.

5.14. Checkerboard assays to determine FIC index

The synergistic activities of antibiotics or antagonistic activities of phospholipids combined with SK-Ps were determined by checkerboard assays with 2-fold serially diluted concentrations in final volumes of 200 μL. Antibacterial drugs or phospholipids were diluted along the ordinate, while SK-Ps were diluted along the abscissa. Then bacterial suspensions in MHB containing approximately 1×10^6 CFU/mL were added. After 16−20 h incubation at 37 °C, the MIC values were defined as the lowest concentrations of antibiotics with no visible growth of bacteria. At least two biological replicates were performed for each combination. Synergy is defined as an FIC index of <0.5. Antagonism is defined as an FIC index of >0.5.

5.15. SEM analysis

Bacterial cultures of *S. aureus* ATCC 29213 at the exponential phase in BHI (CM917B, Beijing Land Bridge Technology) were collected and resuspended into PBS and then treated with SK-P1 for 30 min. Then, bacteria were collected and fixed in a 2.5% glutaraldehyde solution. After fixation, samples were washed with 0.1 mol/L PBS and dehydrated by 30%, 50%, 70%, 80%, 90%, 95%, and 100% (*v*/*v*, in water) EtOH for analysis by SEM (JSM-7900F, JEOL Ltd., Tokyo, Japan).

5.16. Preparation of 5-carboxyfluorescein encapsulated liposomes and fluorescence leakage assay

The POPG liposomes were prepared by the thin-film hydration method[59]. Briefly, 10 mg POPG (1-palmitoyl-2-oleoyl-sn-glycero-3-phosphorylglycerol sodium salt, Merck & Co. Inc., Darmstadt, Germany) was dissolved in 1 mL of a $CHCl_3$/MeOH (1:1) solution and dried to form a lipid film at the bottom of the glass tube. Then, the lipid films were hydrated with ultrapure water (3 mL) with 0.33 mg/mL 5-carboxyfluorescein (Merck) and sonicated for 30 min to form liposomes. The untrapped carboxyfluorescein was separated with ultrafiltration. To determine the leakage of 5-carboxyfluorescein, different peptaibols (20 μg/mL) were added to the liposome, and the final concentration of 1% Triton X-100 was added to promote full fluorescence leakage. The fluorescence was measured at the excitation wavelength of 492 nm and emission wavelength of 518 nm in 2-min intervals using the Infinite M200 Microplate reader (Tecan). The percentage of 5-carboxyfluorescein leakage was determined as Eq. (1):

$$\text{Leakage}_{(t)}\ (\%) = [(I_{(t)} - I_0)/(I_{\text{total}} - I_0)] \times 100 \quad (1)$$

where I_0 is the initial fluorescence, before adding peptide, and I_{total} is the maximum fluorescence, obtained after the addition of Triton X-100.

5.17. ITC assay

Calorimetric experiments were performed to evaluate the interaction between POPG and SK-Ps by PEAQ ITC (Malvern Panalytical Ltd., Almelo, Netherlands) at 25 °C. To determine the affinity between SK-Ps and PG, both 2 mmol/L of POPG and 0.2 mmol/L of SK-Ps were dissolved in 10−30% (*v*/*v*, in water) methanol. Sequential injections of PG into the calorimetric cell filled with SK-Ps were repeated 19 times with equilibration intervals of 200 s. The obtained data were processed using the software with the instrument to calculate the equilibrium dissociation constant (K_D), stoichiometry (n), and changes of enthalpy (ΔH) and entropy (ΔS).

5.18. Bacterial membrane integrity assay

An overnight cultured *S. aureus* ATCC 29213 growing from a single colony in BHI broth was washed and resuspended in 0.01 mol/L of PBS (pH 7.4) to obtain an OD_{600} of 0.5, followed by the addition of propidium iodide (PI, Merck) to a final concentration of 5 μmol/L. Then the 190 μL of the mixture was added to a 96-well plate treated with 10 μL of SK-P1 at the levels of 1, 5, and 10 μg/mL. Nisin (100 μg/mL) was used as positive control. The fluorescence was measured at the excitation wavelength of 535 nm and emission wavelength of 615 nm in 2-min intervals using the Infinite M200 Microplate reader (Tecan, Mannedorf, Switzerland).

5.19. Δψ, ΔpH and ROS measurement

An overnight cultured *S. aureus* ATCC 29213 in BHI broth was washed and resuspended in 5 mmol/L of HEPES (pH 7.0, +5 mmol/L of glucose, Merck) to obtain an OD_{600} of 0.5. Then a fluorescent probe 3,3-dipropylthiadicarbocyanine iodide $DiSC_3(5)$ (Merck) for $\Delta\psi$ measurement, 2′,7′-dichloro-fluorescein diacetate (DCFH-DA, Merck) for ΔpH measurement, BCECF-AM (Merck)

for ROS measurement was added until a final concentration of 10 μmol/L and incubated at 37 °C for 30 min. After washing with HEPES three times, the membrane potential, intracellular pH, and ROS accumulation in the presence and absence of SK-P1 at the levels of 1, 5, and 10 μg/mL were measured using the Infinite M200 Microplate reader (Tecan).

5.20. ATP determination

ATP levels were determined using an Enhanced ATP Assay Kit (S0027, Beyotime, Shanghai, China). Cultured *S. aureus* ATCC 29213 was washed and resuspended to obtain an OD_{600} of 0.5 with 0.01 mol/L of PBS (pH 7.4). After treatment with SK-P1 (1, 5, and 10 μg/mL) at 37 °C for 1 h, bacterial cultures were centrifuged at 4 °C and the supernatants were collected for the detection of extracellular ATP levels. The remaining bacterial precipitates were lysed by lysostaphin at 37 °C for 20 min. After centrifugation, the supernatants were prepared for the measurement of intracellular ATP levels. Last, the supernatants were added to the well to detect the solution before recording in the model of luminescence using the Infinite M200 Microplate reader (Tecan).

5.21. Cytotoxicity assay

Haca T, IEC-6, and A549 cells were cultured in DMEM medium, which contained 1% FBS. Cells were seeded in 96-well plates (1×10^4 cells/200 μL) and incubated with different concentrations of SK-P2 for 24 h. A volume of 100 μL of fresh medium containing 10 μL of WST-1 (Roche, Germany) solution was added to each well after the removal of the cell medium, and the cells were incubated at 37 °C for 1 h. The absorption of the samples was measured on a microplate reader (Tecan) at 450 nm. Cell viability (IC_{50}) was determined by the concentrations of analytes with 50% inhibition of cell growth.

5.22. Galleria mellonella infection model

The model was constructed based on our previous study[60]. The larvae of *G. mellonella* (Tianjin Huiyude Biotech Company, Tianjin, China) were randomly divided into three groups ($n = 7$ per group) and infected with 10 μL of MRSA T144 suspension (5.0×10^6 CFUs) at the right posterior gastropoda. At 1 h post-infection, *G. mellonella* was treated with PBS (0.01 mol/L, pH = 7.4), vancomycin (10 mg/kg), and SK-P1 (10 mg/kg) at the left posterior gastropoda. Survival rates and bacterial burdens of MRSA of *G. mellonella* larvae were recorded.

5.23. Ethics statement

Female BALB/c mice (6−8 weeks old) were obtained from Beijing Vital River Laboratory, Beijing, China. All mice weighed 18−20 g when tested. Mice adapted to standardized environmental conditions (temperature = 23 ± 2 °C; humidity = 55 ± 10%) for 1 week before infection in China Agricultural University to minimize potential con-founders. Mice were maintained in strict accordance with the regulations for the Administration of Affairs Concerning Experimental Animals approved by the State Council of People's Republic of China (11-14-1988). The animal study protocols were performed following the relevant guidelines and regulations (ID: SKLAB-B-2010−003). The laboratory animal usage license number is AW80013202-2-1, certified by the Beijing Association for Science and Technology.

5.24. Mouse wound infection model

The model was constructed based on our previous study[60]. Mice ($n = 6$ per group, 18 mice were used in total) were anesthetized (pentobarbital sodium, 50 mg/kg), and then 10 mm diameter wounds were created on their backs using surgical punches. After that, a suspension containing 1×10^7 CFU MRSA T144 in PBS (0.01 mol/L, pH = 7.4) was inoculated onto each wound. At 1 h post-infection, 10 mg/kg SK-P1 or vancomycin was topically administered to each wound. Vancomycin (10 mg/kg) was used as a positive control, and the PBS (0.01 mol/L, pH = 7.4) group was used as a negative control. The gross appearance of the skin surface was monitored for 12 days. At the end of the experiment, the wound skin was excised for homogenization to count the concentration of TNF-α, IL-6, and bacterial burdens of MRSA.

Acknowledgments

This work was supported by National Key Research and Development Program of China (2022YFD1801600, 2022YFC2804900), National Natural Science Foundation of China (81991525, 32230106), China Postdoctoral Science Foundation (2022M710266).

Author contributions

Shang Chen: Writing − original draft, Visualization, Methodology, Investigation, Funding acquisition. Dong Liu: Visualization, Methodology, Investigation. Liyang Wang: Visualization, Methodology. Aili Fan: Methodology, Funding acquisition. Mengyue Wu: Methodology. Ning Xu: Methodology. Kui Zhu: Writing − review & editing, Supervision, Funding acquisition, Conceptualization. Wenhan Lin: Writing − review & editing, Supervision, Resources, Funding acquisition, Conceptualization.

Conflicts of interest

The authors declare no conflicts of interest.

Appendix A. Supporting information

Supporting information to this article can be found online at https://doi.org/10.1016/j.apsb.2025.02.036.

References

1. Murray CJL, Ikuta KS, Sharara F, Swetschinski L, Robles Aguilar G, Gray A, et al. Global burden of bacterial antimicrobial resistance in 2019: a systematic analysis. *Lancet* 2022;**399**:629−55.
2. Liu YY, Wang Y, Walsh TR, Yi LX, Zhang R, Spencer J, et al. Emergence of plasmid-mediated colistin resistance mechanism MCR-1 in animals and human beings in China: a microbiological and molecular biological study. *Lancet Infect Dis* 2016;**16**:161−8.
3. He T, Wang R, Liu DJ, Walsh TR, Zhang R, Lv Y, et al. Emergence of plasmid-mediated high-level tigecycline resistance genes in animals and humans. *Nat Microbiol* 2019;**4**:1450−6.
4. Lewis K. Platforms for antibiotic discovery. *Nat Rev Drug Discov* 2013;**12**:371−87.
5. Lewis K. The science of antibiotic discovery. *Cell* 2020;**181**:29−45.

6. Liu MM, El-Hossary EM, Oelschlaeger TA, Donia MS, Quinn RJ, Abdelmohsen UR. Potential of marine natural products against drug-resistant bacterial infections. *Lancet Infect Dis* 2019;**19**:e237.
7. Xu ZL, Liu DY, Liu D, Ren X, Liu HB, Qi GH, et al. Equisetin is an anti-obesity candidate through targeting 11β-HSD1. *Acta Pharm Sin B* 2022;**12**:2358−73.
8. Rao Y, Su R, Wu CY, Chai XX, Li JJ, Yang GY, et al. Identification of a natural PLA2 inhibitor from the marine fungus *Aspergillus* sp. c1 for MAFLD treatment that suppressed lipotoxicity by inhibiting the IRE-1α/XBP-1s axis and JNK signaling. *Acta Pharm Sin B* 2024;**14**:304−18.
9. Zan JD, Li ZY, Tianero MD, Davis J, Hill RT, Donia MS. A microbial factory for defensive kahalalides in a tripartite marine symbiosis. *Science* 2019;**364**:e6732.
10. Ma JY, Huang HB, Xie YC, Liu ZY, Zhao J, Zhang CY, et al. Biosynthesis of ilamycins featuring unusual building blocks and engineered production of enhanced anti-tuberculosis agents. *Nat Commun* 2017;**8**:e391.
11. Willems T, De Mol ML, De Bruycker A, De Maeseneire SL, Soetaert WK. Alkaloids from marine fungi: promising antimicrobials. *Antibiotics* 2020;**9**:340.
12. Karpiński TM. Marine macrolides with antibacterial and/or antifungal activity. *Mar Drugs* 2019;**17**:e241.
13. Wu B, Wiese J, Wenzel-Storjohann A, Malien S, Schmaljohann R, Imhoff JF. Engyodontochones, antibiotic polyketides from the marine fungus *Engyodontium album* strain LF069. *Chem-eur J* 2016;**22**: 7452−62.
14. Dieterich CL, Probst SI, Ueoka R, Sandu I, Schäfle D, Molin MD, et al. Aquimarins, peptide antibiotics with amino-modified *c*-termini from a sponge-derived *Aquimarina* sp. bacterium. *Angew Chem Int Edit* 2022;**61**:e202115802.
15. Valdes-Pena MA, Massaro NP, Lin Y, Pierce JG. Leveraging marine natural products as a platform to tackle bacterial resistance and persistence. *Acc Chem Res* 2021;**54**:1866−77.
16. Liu Y, Ding SY, Shen JZ, Zhu K. Nonribosomal antibacterial peptides that target multidrug-resistant bacteria. *Nat Prod Rep* 2019;**36**:573−92.
17. Wang ZQ, Forelli N, Hernandez Y, Ternei M, Brady SF. Lapcin, a potent dual topoisomerase I/II inhibitor discovered by soil metagenome guided total chemical synthesis. *Nat Commun* 2022;**13**:e842.
18. Bayer AS, Schneider T, Sahl HG. Mechanisms of daptomycin resistance in *Staphylococcus aureus*: role of the cell membrane and cell wall. *Ann NY Acad Sci* 2013;**1277**:139−58.
19. Shukla R, Peoples AJ, Ludwig KC, Maity S, Derks MGN, De Benedetti S, et al. An antibiotic from an uncultured bacterium binds to an immutable target. *Cell* 2023;**186**:4059−73.
20. Wang ZQ, Koirala B, Hernandez Y, Zimmerman M, Park S, Perlin DS, et al. A naturally inspired antibiotic to target multidrug-resistant pathogens. *Nature* 2022;**601**:606−11.
21. Culp EJ, Waglechner N, Wang WL, Fiebig-Comyn AA, Hsu Y, Koteva K, et al. Evolution-guided discovery of antibiotics that inhibit peptidoglycan remodelling. *Nature* 2020;**578**:582−7.
22. Chugh JK, Wallace BA. Peptaibols: models for ion channels. *Biochem Soc Trans* 2001;**29**:565−70.
23. Duclohier H, Wróblewski H. Voltage-dependent pore formation and antimicrobial activity by alamethicin and analogues. *J Membr Biol* 2001;**184**:1−12.
24. Lin LM, Chi JY, Yan YL, Luo R, Feng XQ, Zheng YW, et al. Membrane-disruptive peptides/peptidomimetics-based therapeutics: promising systems to combat bacteria and cancer in the drug-resistant era. *Acta Pharm Sin B* 2021;**11**:2609−44.
25. Stachelhaus T, Mootz HD, Marahiel MA. The specificity-conferring code of adenylation domains in nonribosomal peptide synthetases. *Chem Biol* 1999;**6**:493−505.
26. Liu D, Lin H, Proksch P, Tang XX, Shao ZZ, Lin WH. Microbacterins A and B, new peptaibols from the deep sea actinomycete *Microbacterium sediminis* sp. nov. YLB-01(T). *Org Lett* 2015;**17**:1220−3.
27. Long HL, Cheng ZB, Huang W, Wu Q, Li XD, Cui JR, et al. Diasteltoxins A−C, asteltoxin-based dimers from a mutant of the sponge-associated *Emericella variecolor* Fungus. *Org Lett* 2016;**18**:4678−81.
28. Blin K, Shaw S, Augustijn HE, Reitz ZL, Biermann F, Alanjary M, et al. antiSMASH 7.0: new and improved predictions for detection, regulation, chemical structures and visualisation. *Nucleic Acids Res* 2023;**51**:W46−50.
29. Brückner H, Przybylski M. Isolation and structural characterization of polypeptide antibiotics of the peptaibol class by high-performance liquid chromatography with field desorption and fast atom bombardment mass spectrometry. *J Chromatogr A* 1984;**296**:263−75.
30. Rinehart Jr KL, Gaudioso LA, Moore ML, Pandey RC, Cook Jr JC, Barber M, et al. Structures of eleven zervamicin and two emerimicin peptide antibiotics studied by fast atom bombardment mass spectrometry. *J Am Chem Soc* 1981;**103**:6517−20.
31. Mohamed-Benkada M, Montagu M, Biard JF, Mondeguer F, Verite P, Dalgalarrondo M, et al. New short peptaibols from a marine *Trichoderma* strain. *Rapid Commun Mass Sp* 2006;**20**:1176−80.
32. Auvin-Guette C, Rebuffat S, Prigent Y, Bodo B. Trichogin A IV, an 11-residue lipopeptaibol from *Trichoderma longibrachiatum*. *J Am Chem Soc* 1992;**114**:2170−4.
33. Ritzau M, Heinze S, Dornberger K, Berg A, Fleck W, Schlegel B, et al. Ampullosporin, a new peptaibol-type antibiotic from *Sepedonium ampullosporum* HKI-0053 with neuroleptic activity in mice. *J Antibiot* 1997;**50**:722−8.
34. Tsantrizos YS, Pischos S, Sauriol F, Widden P. Peptaibol metabolites of *Tolypocladium geodes*. *Can J Chem* 1996;**74**:165−72.
35. Chikanishi T, Hasumi K, Harada T, Kawasaki N, Endo A. Clonostachin, a novel peptaibol that inhibits platelet aggregation. *J Antibiot* 1997;**50**:105−10.
36. Fujita T, Takaishi Y, Okamura A, Fujita E, Fuji K, Hiratsuka N, et al. New peptide antibiotics, trichopolyns I and II, from *Trichoderma polysporum*. *J Chem Soc , Chem Commun* 1981:585−7.
37. Du L, Risinger AL, Mitchell CA, You JL, Stamps BW, Pan N, et al. Unique amalgamation of primary and secondary structural elements transform peptaibols into potent bioactive cell-penetrating peptides. *Proc Natl Acad Sci USA* 2017;**114**:E8957−66.
38. Kredics L, Szekeres A, Czifra D, Vágvölgyi C, Leitgeb B. Recent results in alamethicin research. *Chem Biodivers* 2013;**10**:744−71.
39. Su ZF, Leitch JJ, Lipkowski J. Effect of lipid composition on the inhibition mechanism of amiloride on alamethicin ion channels in supported phospholipid bilayers. *Langmuir* 2022;**38**:8398−406.
40. MacNair CR, Brown ED. Outer membrane disruption overcomes intrinsic, acquired, and spontaneous antibiotic resistance. *mBio* 2020; **11**:e01615.
41. MacNair CR, Stokes JM, Carfrae LA, Fiebig-Comyn AA, Coombes BK, Mulvey MR, et al. Overcoming *mcr-1* mediated colistin resistance with colistin in combination with other antibiotics. *Nat Commun* 2018;**9**:e458.
42. Song MR, Liu Y, Li TT, Liu XJ, Hao ZH, Ding SY, et al. Plant natural flavonoids against multidrug resistant pathogens. *Adv Sci* 2021;**8**: e2100749.
43. Yang ZQ, Song MR, Li XY, Zhang Q, Shen JZ, Zhu K. Synergy of outer membrane disruptor SLAP-S25 with hydrophobic antibiotics against Gram-negative pathogens. *J Antimicrob Chemoth* 2022;**78**:263−71.
44. Mileykovskaya E, Dowhan W. Role of membrane lipids in bacterial division-site selection. *Curr Opin Microbiol* 2005;**8**:135−42.
45. Renner LD, Weibel DB. MinD and MinE interact with anionic phospholipids and regulate division plane formation in *Escherichia coli*. *J Biol Chem* 2012;**287**:38835−44.
46. Song MR, Liu Y, Huang XY, Ding SY, Wang Y, Shen JZ, et al. A broad-spectrum antibiotic adjuvant reverses multidrug-resistant Gram-negative pathogens. *Nat Microbiol* 2020;**5**:1040−50.
47. Hilton KLF, Manwani C, Boles JE, White LJ, Ozturk S, Garrett MD, et al. The phospholipid membrane compositions of bacterial cells,

cancer cell lines and biological samples from cancer patients. *Chem Sci* 2021;**12**:13273−82.
48. Hernandez-Villa L, Manrique-Moreno M, Leidy C, Jemiola-Rzeminska M, Ortiz C, Strzalka K. Biophysical evaluation of cardiolipin content as a regulator of the membrane lytic effect of antimicrobial peptides. *Biophys Chem* 2018;**238**:8−15.
49. Bolosov IA, Panteleev PV, Sychev SV, Sukhanov SV, Mironov PA, Myshkin MY, et al. Dodecapeptide cathelicidins of cetartiodactyla: structure, mechanism of antimicrobial action, and synergistic interaction with other cathelicidins. *Front Microbiol* 2021;**12**:e725526.
50. Song MR, Chen S, Lin WH, Zhu K. Targeting bacterial phospholipids and their synthesis pathways for antibiotic discovery. *Prog Lipid Res* 2024;**96**:101307.
51. Grein F, Muller A, Scherer KM, Liu XL, Ludwig KC, Klockner A, et al. Ca^{2+}-daptomycin targets cell wall biosynthesis by forming a tripartite complex with undecaprenyl-coupled intermediates and membrane lipids. *Nat Commun* 2020;**11**:e1455.
52. Moreira R, Taylor SD. Establishing the structure-activity relationship between phosphatidylglycerol and daptomycin. *ACS Infect Dis* 2022;**8**: 1674−86.
53. Lv BY, Huang XB, Lijia CC, Ma YL, Bian MM, Li ZY, et al. Heat shock potentiates aminoglycosides against gram-negative bacteria by enhancing antibiotic uptake, protein aggregation, and ROS. *Proc Natl Acad Sci USA* 2023;**120**:e2217254120.
54. Stokes JM, Yang K, Swanson K, Jin WG, Cubillos-Ruiz A, Donghia NM, et al. A deep learning approach to antibiotic discovery. *Cell* 2020;**180**:688−702.
55. Kohanski MA, Dwyer DJ, Hayete B, Lawrence CA, Collins JJ. A common mechanism of cellular death induced by bactericidal antibiotics. *Cell* 2007;**130**:797−810.
56. Su JJ, Li HM, Hu JY, Wang DN, Zhang FC, Fu Z, et al. LcCCL28-25, derived from piscine chemokine, exhibits antimicrobial activity against Gram-negative and Gram-positive bacteria *in vitro* and *in vivo*. *Microbiol Spect* 2022;**10**:e02515.
57. Tsai CJ, Loh JMS, Proft T. *Galleria mellonella* infection models for the study of bacterial diseases and for antimicrobial drug testing. *Virulence* 2016;**7**:214−29.
58. De Zotti M, Biondi B, Crisma M, Hjørringgaard CU, Berg A, Brückner H, et al. Isovaline in naturally occurring peptides: a nondestructive methodology for configurational assignment. *Pept Sci* 2012;**98**:36−49.
59. Chen YX, Xing Y, Han JH, Liu SH, Xiang X, Shen JZ, et al. Multifunctional MMP9-responsive silicasomes-GelMA hydrogels with bacteria-targeting capability and tissue restoration function for chronic wound infection. *Chem Eng J* 2023;**475**:e146246.
60. Chen S, Liu D, Zhang Q, Guo P, Ding SY, Shen JZ, et al. A marine antibiotic kills multidrug-resistant bacteria without detectable high-level resistance. *ACS Infect Dis* 2021;**7**:884−93.